

# Simulation of Automotive Radar Target Lists considering Clutter and Limited Resolution

Markus Bühren and Bin Yang  
Chair of System Theory and Signal Processing  
University of Stuttgart, Germany  
*www.LSS.uni-stuttgart.de*

**Abstract**—In the field of automotive radar signal processing, often real data is used from the beginning in the development of algorithms, even if simulated data offers several advantages, for example providing an exact reference and allowing to reduce the number of measurement campaigns. However, a radar simulation, for example based on a ray-tracing model, is very complex to implement and needs extremely large computational resources.

In [1]–[3], we have introduced a simulation model for automotive radar target lists that is able to run in real-time on an up-to-date personal computer. The simulation imitates the 24 GHz near-range Pulse-Doppler radar sensor as described in [4], but can be adjusted to other sensors with similar resolution capabilities. In this paper, we present two extensions to the existing model. The first extension improves the simulation of the sensor’s resolution capabilities in situations where two targets at the same distance and Doppler velocity melt into a single phantom target. The second new module considers the radar clutter *before* the sensor-internal tracking.

## I. REVIEW OF THE SIMULATION MODEL

In order to build a radar target list simulation model, we have reviewed a large amount of real radar measurements. Our experience shows that the reflections of an object vehicle mainly stem from the four vehicle corners and the four wheel houses. Further, the car body reflects radar energy if it impinges perpendicular. These observations lead to a representation of a vehicle by eight point reflection centers and four plane reflectors, as described in detail in [1] and [2].

While we have designed this model based on our experience with real radar data, in [5] a similar model has been derived by performing a ray-tracing simulation and clustering the resulting reflection points. In [6], again a point reflector model is derived. But both models do not include plane reflectors which help to

provide more realistic results in certain situations and to reduce the computational effort of the simulation.

Based on the reflection center model of objects, an *ideal target list* in bearing, range and Doppler velocity can be computed by geometrical considerations for a given traffic situation. With the term ideal target list we refer to a target list that would be returned by a hypothetical sensor without any measurement noise and unlimited resolution.

The ideal target list is independent of the specific type of sensor. It is transformed into a realistic target list by applying a specific sensor model. In our case, we are dealing with a model of the automotive radar sensor in [4].

In the sensor model, first the measured amplitude is computed by considering distance, antenna pattern, object RCS and multipath propagation [3]. If this amplitude exceeds a certain threshold, a target is said to be detected. In sections II and III, we will present how the sampling and detection is done in a real sensor and how it can be simulated realistically but with low computational effort.

The real data sets we have been using so far in the design of the simulation model were recorded with the internal tracking switched on and included practically no clutter at all. However, as we recently had the chance to record data with the internal tracking switched off in a special software configuration, we decided to extend the model to simulate both the pre-tracked final sensor output and the intermediate measurements before the sensor-internal tracking. In sections IV and V, we will present the analysis and simulation of clutter caused by ground reflections.

## II. SAMPLING AND DETECTION

The procedure of sending pulses and sampling the echoes in a typical automotive radar sensor is very well described in [7]. For each distance cell,

a number of pulses (e.g. 128 or 1024) is transmitted, received, downmixed, quadrature-modulated and sampled. The complex samples ( $I/Q$ ) are then transformed into a Doppler spectrum using the FFT. For each distance-velocity- or  $R$ - $v$ -cell, a complex FFT value results. The detection is usually done in the Doppler domain, where the FFT magnitudes are compared to an adaptive threshold. All FFT values that exceed the threshold are candidates for being caused by real objects.

For the angle estimation using the sequential lobing principle [4], two different antenna patterns are used and the so-called additive sensing ratio is computed. If there are two objects present in a single  $R$ - $v$ -cell, but at different angles (e.g. two vehicles with equal velocity driving ahead on different lanes), the contributions of both targets superimpose and can not be distinguished. The result of the angle estimation will be a single angle, typically in the middle between the targets.

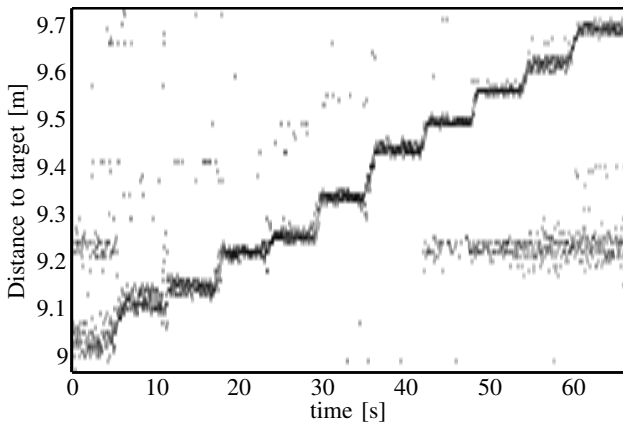


Fig. 1. Target distance measurements over time

For tracking algorithms that process the radar signals to form an object list, it is important to take this “angle error” into account. Thus a simulation, which is used for algorithm development, has to represent the melting of targets realistically. In the following section we present how the sampling and interpolation in distance is reflected in our simulation. First, however, the real radar measurements which form the basis of our simulation development are discussed.

In one measurement experiment, we used two corner reflectors as targets. One was standing straight ahead of the observing vehicle, while the other reflector was positioned a little closer to the sensor in an angle of about  $24^\circ$  to the left. We moved the second reflector in steps of some centimeters away from

the sensor, so that both reflectors were lying in the same  $R$ - $v$ -cell during the middle of the measurement experiment.

In Fig. 1, the distance measurements are displayed over the time. Every column of the displayed image represents a histogram of the distance values. The detections forming a staircase are those caused by the moving corner reflector. At a distance of about 9.22 m, there are detections of the static reflector visible at the beginning and the end of the measurement. In the middle, the two targets can not be separated and thus only the staircase can be seen. The distance resolution in this particular case can be derived from this measurement. At around 45 s, the distance of the two targets differs by 26 cm and the targets can just be separated, so the resolution is approximately equal to this distance.

The amplitude measurements of the same data set are plotted over the measured distance in Fig. 2. The measurements are quantized with 2 dB in amplitude and 1 cm in distance. For a better visibility, we added uniform noise between  $-0.75$  and  $0.75$  dB in amplitude and between  $-2.5$  and  $2.5$  mm in distance before plotting. The time is encoded by the gray level: the darkest dots are from the beginning of the measurement, the detections shown in lighter gray level were recorded later. The vertical lines mark the positions where the stepwise moving reflector was standing (compare to the staircase levels in Fig. 1).

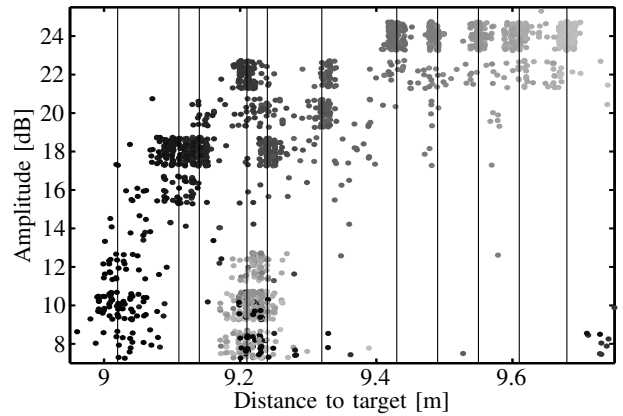


Fig. 2. Target amplitudes over distance

The detections of the standing corner reflector are lying between about 9.1 and 9.3 m and below 14 dB. Here, some very dark dots and many light dots are visible, but no dots with an intermediate gray level. This confirms the observation of Fig. 1, where there are no detections of the standing reflector visible in the middle of the measurement.

The remaining amplitude values are those caused by the moving reflector. The reason for the increase of the amplitude from below 10 up to 24 dB with increasing distance is multipath propagation. As the road surface acts as a reflector for the radar waves, different propagation path from sensor to object exist. As analyzed in detail in [3], the different delays on the different paths cause severe interference effects that can even lead to nearly complete cancellation. In our measurement experiment, the moving corner reflector was (unintentionally) placed into a rising edge of the interference pattern.

As the amplitudes of the two reflectors are quite different, the resolution value derived above from Fig. 1 is only applicable in this particular case. If the reflectors were placed at different positions of the interference pattern, a different behavior might result. However, as the resolution is mainly determined by the pulse width, similar values can be expected.

### III. MODEL OF SAMPLING AND DETECTION

In the following, we will describe how the sampling and detection is represented in our simulation model. One possible way would be to generate complex samples based on the ideal targets list for every single received pulse. However, this would mean a very large computational effort. Instead, we apply some simplifications – without losing much accuracy – and only simulate a small number of samples.

In our measurement experiment introduced in the last section, it was possible to create a scenario where two objects had the same relative velocity (0 m/s) and reached the same distance during the measurement by moving a corner reflector step by step. Based on this data we can conclude about the resolution in distance. The creation of a scenario where we can estimate the resolution in relative velocity would need much more effort and was not realized during this work. Due to this, we do an abstraction of the resolution capability in relative velocity. If two entries in the ideal target list differ less than a threshold in relative velocity, they are marked as candidates for melting into a single target, otherwise not. The threshold was chosen to 0.12 m/s based on our experience with other measurements.

In the simulation, we next check which of the ideal target list entries with similar relative velocity are closer than 0.6 m in distance. For each of such groups, as well as for single targets, we simulate the (complex) samples in distance dimension. In a range between 15 cm below the minimum true

distance of the involved targets and 15 cm above the maximum true distance, the interesting part is sufficiently covered.

Unfortunately we do not have detailed information about the sensor internals, which makes system identification an integral part of our work. What we know is that the sampling is done on a grid of 5 cm and that an interpolation between three consecutive samples is done in order to estimate the target distance.

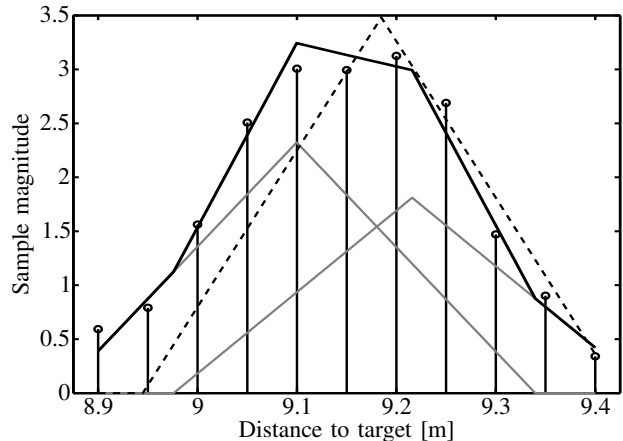


Fig. 3. Simulated samples

For the sampling simulation, we need the pulse form and width. A Gaussian-shaped pulse offers the advantage of an optimal time-bandwidth-product. However, forming Gaussian-shaped pulses requires some technical effort in the radar sensor. Thus we assume that in favor of reduced production costs, rectangular-shaped pulses are realized by switching the HF-energy on and off very quickly [7]. The pulses after the receiving matched filter will then have triangular shape. Due to limited bandwidth in transmitter and receiver and non-ideal switches, the pulse form will not be ideally triangular, but something in between a triangular and a Gaussian pulse. However, we use triangular pulses in the simulation, expecting that the results will not be affected very much by the exact pulse form. The radar bandwidth is known to be 5 GHz, thus the pulse width has to be around 200 ps.

In Fig. 3, a snapshot of the samples in a situation with two close targets is shown. The ideal pulse forms of the targets are represented by the gray lines, the sum of these by the solid black line. The pulse amplitudes have been determined before in the simulation, considering antenna patterns, multipath propagation etc. [3]. The circles in Fig. 3 mark the simulated samples, i.e. the absolute values of the ideal pulse form plus artificial, complex noise. The

variance of the noise has been derived by comparing real and simulated data sets.

After the simulation of the noisy samples, the next step is to find the relative maxima that exceed a detection threshold. They are then worked through in decreasing order of magnitude. For each relative maximum, the distance is estimated by considering the maximum sample and the samples left and right of it. For the interpolation, different approaches are possible, for example fitting a parabola that passes through all three points and using the maximum of this parabola as the distance estimation. As we know the exact pulse form, here we use a least-squares fit of a triangular pulse with fixed width. The result is shown in Fig. 3 as dashed line. The interpolation allows a distance accuracy significantly below the size of the distance cells.

In all real measurements with the internal tracking switched off, we observed that two returned targets with the same relative velocity were always at least 15 cm separated in distance. We conclude that this is a limit set explicitly in the detection algorithm. Otherwise, relative maxima that are very close to each other and are caused only by the noise (like the one at 9.1 m in Fig. 3) would be returned as separate targets. Thus also in our simulation, after doing the distance interpolation for one relative maximum, we only proceed if the other maxima are at least 15 cm away from the current one.

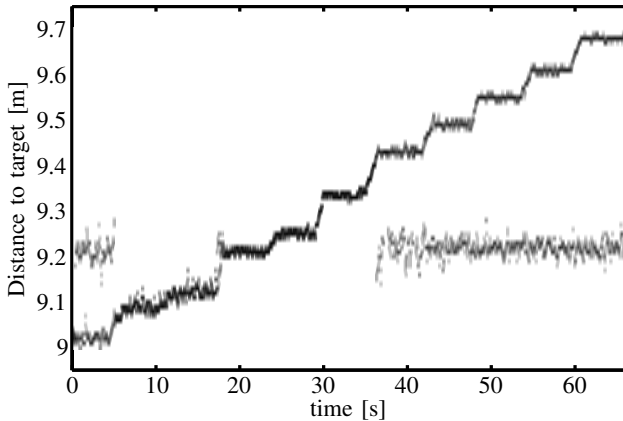


Fig. 4. Simulated target distance measurements over time

At this point, noisy target distance measurements were simulated by the interpolation of noisy samples. For the relative velocity, a weighted average of the true relative velocities of all targets that contribute to the current detection is used. In order to simulate measurement noise, we add artificial noise with a variance that depends linearly on the simulated

amplitude in dB, a relation that was derived from real data of other measurement experiments. For the amplitude, we use the height of the least-squares-fitted triangular pulse.

Finally, the bearing angle has to be estimated. This is done, as mentioned before, by the sequential lobing method [1]. The samples simulated so far were those received with the sum antenna diagram. For the angle estimation, we use the relative maximum sample of the sum diagram and additionally simulate a noisy complex sample of the delta diagram. These two noisy samples are forwarded to the angle estimation, which results in realistic statistical errors and realistic angle errors when two or more targets are in the same  $R$ - $v$ -cell.

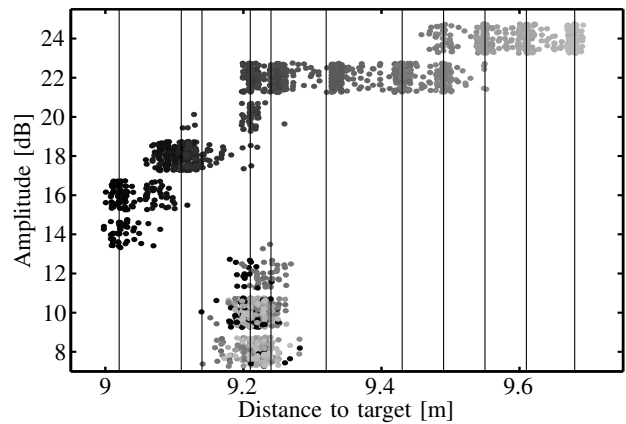


Fig. 5. Simulated target amplitudes over distance

The statistical errors in the relative velocity were modeled explicitly by adding artificial noise of a given variance. The only other noise that we inserted was the complex noise on the simulated samples. It is important to note that this single source of noise generates realistic noise variances (comparing real and simulated data) in three different dimensions: distance, bearing angle and amplitude. This fact is a strong argument of justification for our simulation model, even if some sensor internals might not be modeled absolutely correct.

For a comparison of simulated data with the real measurements, we simulated the situation of our measurement experiment described in section II. The resulting distance measurements are shown in Fig. 4, their real counterparts have been presented in Fig. 2 before. As can be seen, the agreement between real and simulated data is good. Deviations are visible in the regions around 10 and 40 s. Here, the distance resolution in the simulation seems to be a bit too good. The sparse detections that are visible above

the staircase in the real measurements in Fig. 2 are caused by the person moving the corner reflector, who was not considered in the simulation scenario.

Also the amplitudes are simulated realistically, as can be seen in Fig. 5. In the region around the first vertical line at about 9 m, the simulated detections are much stronger than the real ones. This only indicates that the simulated and the real interference patterns do not perfectly agree.

#### IV. CLUTTER ANALYSIS

In Fig. 6, the measured distances of two sensors in an experiment with sensor-internal tracking switched off are shown as dots. The two decreasing lines mark the region where the detections of a corner reflector, which was used as target for other purposes, had to be removed. The remaining detections are all caused by spurious ground reflections and are the basis of our clutter analysis. During the measurements, the ground was wet. A comparison with data sets recorded in different weather conditions was not possible during this work.

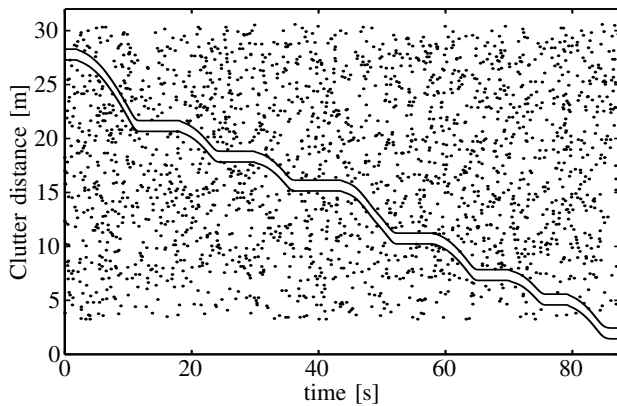


Fig. 6. Clutter targets over distance

A clutter detection occurs if the detection threshold is randomly exceeded. In every of the many  $R$ - $v$ -cells, a clutter detection will occur with a very small probability. Thus the rare occurrence of clutter can be modeled as a Poisson process. A histogram of the number of clutter targets per cycle is shown in Fig. 7. Applying a  $\chi^2$ -test of level 0.03 confirms that this discrete distribution is indeed similar to a Poisson distribution with parameter  $\lambda = 0.62$ .

The distribution of the clutter distance values can roughly be seen in Fig. 6. Below a minimum distance of about 2.9 m, not a single clutter detection is visible. This can be explained by the focusing of the radar sensor in elevation direction. Below a certain

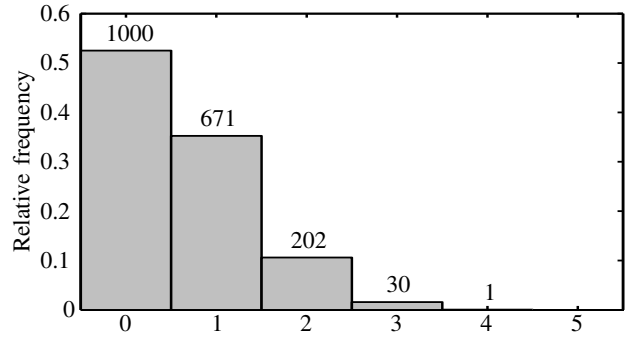


Fig. 7. Histogram of number of clutter targets per cycle

distance, nearly no radar energy will hit the ground. For larger distances, the distribution of the clutter target distances is nearly uniform.

In Fig. 8, a histogram of the measured clutter angles is shown. In the main direction there is more clutter than at the edges of the visibility area. The reason for this is that due to the focusing in azimuth direction, more spurious energy will be collected in the main lobe area. The black curve in Fig. 8 is proportional to the squared antenna pattern in azimuth direction, as it can be derived by the information given in [4]. It fits to the histogram quite well, except the significantly large peak at  $0^\circ$ . The peak can be explained by the applied sequential lobing angle estimation method. Here, an amplitude ratio is computed using two switchable antenna diagrams, where the second has a zero at  $0^\circ$ . As the dynamic range of the digital-to-analog-converter is limited, the second antenna diagram will return an amplitude of zero even if the radar target is not exactly at zero direction. This leads to an angle estimation of  $0^\circ$  in a certain region around the main direction.

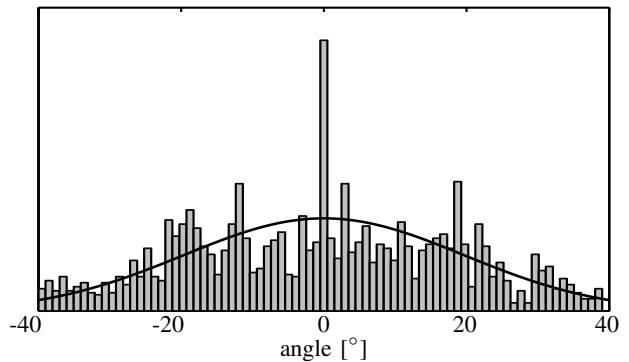


Fig. 8. Histogram of clutter angle

The measured relative velocities of the clutter targets are in good approximation uniformly distributed over the whole range between  $-22$  and  $22$  m/s (due to limited space, we omit a histogram here). As the clutter targets are caused by randomly

exceeding the detection threshold due to the collected spurious energy, there is no reason to expect any other distribution of the measured relative velocity values.

## V. CLUTTER SIMULATION

In this section, we will present how we simulate clutter targets. In the simulation of sampling and detection, as described in section III, no clutter targets will occur, as there are only true reflectors considered. We will add clutter targets to the simulated detections based on the analysis in the last section.

First of all, in every sensor and every measurement cycle, we will draw the number of clutter targets as a random number from a Poisson distribution with parameter  $\lambda = 0.62$ . The first ten probability values ( $n = 0, \dots, 9$ ) of this discrete distribution are given in Table I. The last values are very small and decrease roughly about one order of magnitude from one value to the next. Thus we can approximate the Poisson distribution, which theoretically extends until infinity, by a distribution of limited extension (e.g. until  $n = 5$ ) without noticeable error. This is possible because the parameter  $\lambda$  is very small. A more sophisticated method to generate Poisson random numbers for larger  $\lambda$  is given in [8].

$n = 0$	$n = 1$	$n = 2$	$n = 3$	$n = 4$
0.538	0.334	0.103	0.0214	0.00331
$n = 5$	$n = 6$	$n = 7$	$n = 8$	$n = 9$
4.11 e-4	4.24 e-5	3.76 e-6	2.91 e-7	2.01 e-8

Table I. First probability values of Poisson distribution

After the number of clutter targets was determined, the values of distance, angle and relative velocity for each target are also drawn randomly from continuous distributions and then quantized. For the distance, we use a uniform distribution between the minimum observable clutter distance of 2.9 m and the radar range of 30 m. The PDF of the distribution of angles is approximated by the curve in Fig. 8. The peak at  $0^\circ$  is omitted, as the impact on the consecutive processing and the final target list is very small. Generating random numbers from this distribution is done by drawing a random number from a uniform distribution on  $[0, 1]$  and then using the inverse of the cumulative distribution function (CDF) on this value (so-called inversion method). Finally, another uniform distribution is applied to simulate the relative velocity values between  $-22$  and  $22$  m/s.

The clutter that is simulated as described in this section can nearly completely be removed by a simple data association procedure in the sensor-internal tracking. However, it is important to consider the effect of clutter in this simulation model, as the radar target list processing algorithms being developed with this simulation have to be tested in scenarios as realistically as possible.

## VI. CONCLUSION

In this paper, we have presented extensions to our existing radar target list simulation model. The effect of two or more targets melting to a single phantom target in one  $R$ - $v$ -cell is now well represented by simulating the complex samples that the detection is based on. By simulating the interpolation between several samples in distance, realistic statistical errors in the simulated distance measurements are generated.

The clutter that can be observed *before* the sensor-internal tracking stage has been statistically analyzed. By a simulation model involving only a small number of random generators, clutter can be simulated realistically and in a very efficient way.

## REFERENCES

- [1] Markus Bühren and Bin Yang, "Automotive radar target list simulation based on reflection center representation of objects," in *Proc. Intern. Workshop on Intelligent Transportation (WIT)*, Hamburg, Germany, Mar. 2006, pp. 161–166.
- [2] Markus Bühren and Bin Yang, "Simulation of automotive radar target lists using a novel approach of object representation," in *Proc. IEEE Intelligent Vehicles Symposium*, Tokyo, Japan, June 2006, pp. 314–319.
- [3] Markus Bühren and Bin Yang, "Extension of automotive radar target list simulation to consider further physical aspects," in *Proc. Int. Conf. on ITS Telecommunications (ITST)*, Sophia Antipolis, France, June 2007, pp. 124–129.
- [4] Hermann Henfling, Dirk Klotzbücher and Christian Frank, "Ultra wide band 24GHz sequential lobing radar for automotive applications," in *Proc. Intern. Radar Symposium (IRS)*, Berlin, Germany, Sep. 2005, pp. 79–82.
- [5] Karin Schuler, Rainer Lenz, Denis Becker and Werner Wiesbeck, "Extraction of scattering centers of vehicles by ray-tracing simulations," in *Proc. Intern. Workshop on Intelligent Transportation (WIT)*, Hamburg, Germany, Mar. 2007.
- [6] Lars Mesow, "Multisensorielle Datensimulation im Fahrzeugumfeld für die Bewertung von Sensorfusionsalgorithmen," Dissertation, Technische Universität Chemnitz, Apr. 2006.
- [7] Markus Wintermantel, "High efficient signal processing in a radar based ACC-system," in *Proc. Intern. Radar Symposium (IRS)*, Dresden, Germany, Sep. 2003, pp. 131–136.
- [8] Joachim H. Ahrens and Ulrich Dieter, "Computer generation of Poisson deviates from modified normal distributions," *ACM Transactions on Mathematical Software*, vol. 8, no. 2, pp. 163–179, June 1982.